Cooperative Energy Transfer and Upconversion Luminescence of $Sr_5(PO_4)_3OH:Eu^{3+},Yb^{3+}$ phosphor powders

P.P. Mokoena[1*], B. M. Jaffar[2], H.C. Swart[3], O.M. Ntwaeaborwa[1]
[1]Department of Physics and Earth Sciences, Sol Plaatje University, Kimberley, South Africa
[2]School of Physics, University of the Witwatersrand, Private Bag 3, Johannesburg, South Africa

[3]Department of Physics, Box 339, University of the Free State, Bloemfontein 9300, South Africa

E-mail address: puseletso.mokoena@spu.ac.za

Abstract. In this study, strontium hydroxyapatite ($Sr_5(PO_4)_3OH$) doped with europium (Eu^{3+}) and ytterbium (Yb^{3+}) were successfully synthesized by combustion method. The structural, morphological, and optical properties of the phosphors were determined using X-ray diffraction (XRD), high resolution scanning electron microscopy (HRSEM), energy dispersive X-ray spectroscopy (EDS), and photoluminescence (PL) spectroscopy. XRD data confirmed crystallization of pure hexagonal phase of $Sr_5(PO_4)_3OH$ and HRSEM demonstrated a network of particles with uneven shapes having small bright particles on the surfaces of the larger particles. The EDS analysis confirms that bright particles were dominated by rare earth elements, while darker particles are primarily composed of the host material. Upon UV excitation, prominent orange emission and minor red emission peaks corresponding to Eu^{3+} transitions were observed. The red emission was enhanced significantly upon co-doping with Yb^{3+}, which facilitated non-radiative energy transfer from Ytterbium (Yb^{3+}) to Europium (Eu^{3+}). The enhanced red upconversion luminescence of $Sr_5(PO_4)_3OH:Eu^{3+},Yb^{3+}$ phosphors show promising potential for applications in photodynamic therapy (PDT).

Keywords
$Sr_5(PO_4)_3OH:Eu^{3+},Yb^{3+}$ ions; Phosphors; Energy Transfer; Upconversion luminescence

1. Introduction

The multifunctional inorganic materials have attracted considerable attention due to their wide-ranging prospective uses in the biomedical field, such as drug delivery, sensing, and bioimaging [1]. Inorganic host lattices such as phosphates materials have drawn a significant attention as a host over the years due to their diverse properties, including electric, magnetic, ferroelectric, catalytic, and optical characteristics, along with their strong resistance to heat and moisture. [2]. They have exceptional qualities like crystal structural flexibility, the capacity to incorporate a wide variety of dopant ions, biocompatibility, bioactivity, biodegradability, the lack of immunological, low cytotoxicity and inflammatory reactions [3]. Strontium phosphate ($Sr_5(PO_4)_3OH$) are the ideal nanomaterials due to their inexpensive nature, availability, safety, and environmental benefits [4]. $Sr_5(PO_4)_3OH$ doped with rare earth ions such as Eu^{3+}, Ho^{3+}, Er^{3+}, Tm^{3+}, and Yb^{3+} may generate luminescence that covers from the visible to near-infrared spectrum through an up-conversion process [5]. Rare earth ions upconversion luminescence (UCL) processes depends on the abundant f-electron configurations of rare earth ions at the fundamental intermediate excitation states. They can convert two or more sub-bandgap NIR photons into a single usable above-bandgap photon. Through the decades of research, researchers have discovered that most efficient UCL are from the following rare earth ions: $Er^{3+}/Ho^{3+}/Tm^{3+}$ and Yb^{3+} in which energy transfer upconversion mechanism plays a prominent role [6]. Europium (Eu^{3+}) is commonly used as a red emitting rare earth ion, but it has never been considered an UCL ion in the regime of near infrared (NIR) excitation because it

cannot be directly excited by NIR. It has been found that co-doping with an infrared sensitiser (energy donor) such as Yb^{3+} ion results in the red UC emission of Eu^{3+} ion under NIR excitation. The red UCL of Eu^{3+} is due to the cooperative energy transfer (CET) mechanism from the pairs of Yb^{3+} ions to single Eu^{3+} [7]. This study, report on the UCL and CET of $Sr_5(PO_4)_3OH:Eu^{3+},Yb^{3+}$ phosphor powders. The enhanced red emission can be used in light therapy to activate photosensitizers for treatment of tumour cells.

2. Materials and methodology

$Sr_5(PO_4)_3OH$ co-doped Eu^{3+}/Yb^{3+} phosphor powders were synthesized by combustion process using urea as a fuel. $Sr(NO_3)_2{\cdot}4H_2O$, $NH_4)_2HPO_4$, $Eu(NO_3)_3{\cdot}5H_2O$, $Yb(NO_3)_3{\cdot}6H_2O$ and $CO(NH_2)_2$ were used as precursors. Under complete reaction conditions, the theoretical equation for the formation of $Sr_5(PO_4)_3OH$ is given by:

$$15Sr(NO_3)_2{\cdot}4H_2O + 9(NH_4)_2HPO_4 + 16CH_4N_2O = 3Sr_5(PO_4)_3OH + 16CO_2 + 131H_2O + 40N_2 \quad \text{.....(1)}$$

All starting materials, in stoichiometric quantities, were dissolved in 2 ml of distilled water and rapidly agitated until a thick pasty solution was formed. The solution was kept in a furnace at 600 °C. The solution boiled, dehydrated and decomposed producing combustible gases such as CO_2, NH_3 and H_2O by forming the host material. The combustion ashes were cooled to room temperature and gently grounded using a pestle and mortar yielding a fine powder. The materials synthesized were $Sr_5(PO_4)_3OH$, $Sr_5(PO_4)_3OH:Eu^{3+}$, $Sr_5(PO_4)_3OH:Yb^{3+}$ and $Sr_5(PO_4)_3OH:Eu^{3+},Yb^{3+}$ with different concentrations of Eu^{3+} (1, 2, 3, 5, and 7 mol %), Yb^{3+} (7 mol %), and $Eu^{3+}:Yb^{3+}$ (3:7 mol %). All the powders were annealed at 800 °C in air for 2 hours.

3. Characterization

The phase identification of $Sr_5(PO_4)_3OH$ powder was analysed using a Bruker AXS D8 X-ray Diffraction (XRD) with Cu Kα1 radiation (λ = 1.5406Å) in the 20 - 50° (2θ) range. The functional groups were analysed using Fourier Transform Infrared (FTIR) spectrometer in the range 400 – 2000 cm^{-1}. Particle morphology and corresponding elemental compositions of the phosphors under a vacuum of 9.634×10^{-5} Pa were investigated using a JEOL JSM-7800F thermal field emission scanning electron microscope (FE-SEM) equipped with Oxford Aztec 350 X-Max80 Energy x-ray Dispersive Spectroscopy (EDS). The UV-Visible spectra were evaluated using a Perkin Elmer Lambda 950 UV-Vis spectrometer. The spectrometer was operated in the diffuse reflectance mode in the range 200 -1000 nm. The photoluminescence properties were investigated by using and Cary eclipse fluorescence coupled with monochromatized xenon lamp and the upconversion measurements by photoluminescence (PL) system consisting of a fibre-coupled 980 nm NIR (near infrared) laser as the excitation source, iHR320 Horiba Yvon imaging spectrometer, R943 -02 Hamamatsu Photonics photomultiplier (PMT) detector and a SR830 Standford Research System lock-in amplifier.

4. Results and discussion

4.1 Powder X-ray diffraction analysis

The XRD pattern of $Sr_5(PO_4)_3OH$ powder are shown in Fig. 1(a). The main diffraction peaks of $Sr_5(PO_4)_3OH$ powder are corresponding to standard data referenced by ICDD (International Centre for Diffraction Data) Card No. 00-033-1348, with no trace or impurities or additional phases. The $Sr_5(PO_4)_3OH$ powder crystallizes in a hexagonal structure in the $P6_3/m$ space group [8]. The average crystallite size was 43 ± 2 nm. The sharp and narrow peaks confirm the crystallinity of the powder. Fig. 1(b) shows the crystal structure of $Sr_5(PO_4)_3OH$ drawn by VESTA 3D visualization program referenced by ICSD (Inorganic Crystal Structure Database) Code 9011131. The Sr^{2+} ions are present in two non-equivalent cationic sites Sr(1) and Sr(2). The Sr1 and Sr2 atoms are connected to 8 and 9 oxygen atoms to constitute the distorted Sr(1)O8 and Sr(2)O9 polyhedra, respectively [2]. The Sr(1) and Sr(2) atoms crystallographic site with trigonal symmetry (C_3) is coordinated by nine oxygen atoms from the PO_4^{3-} groups, creating $[Sr(1)O_9]$ clusters. The second Sr(2) site is seven coordinated by six oxygen atoms from the PO_4^{3-} groups and one hydrogen ion inside the hexagonal channels of the structure [8].

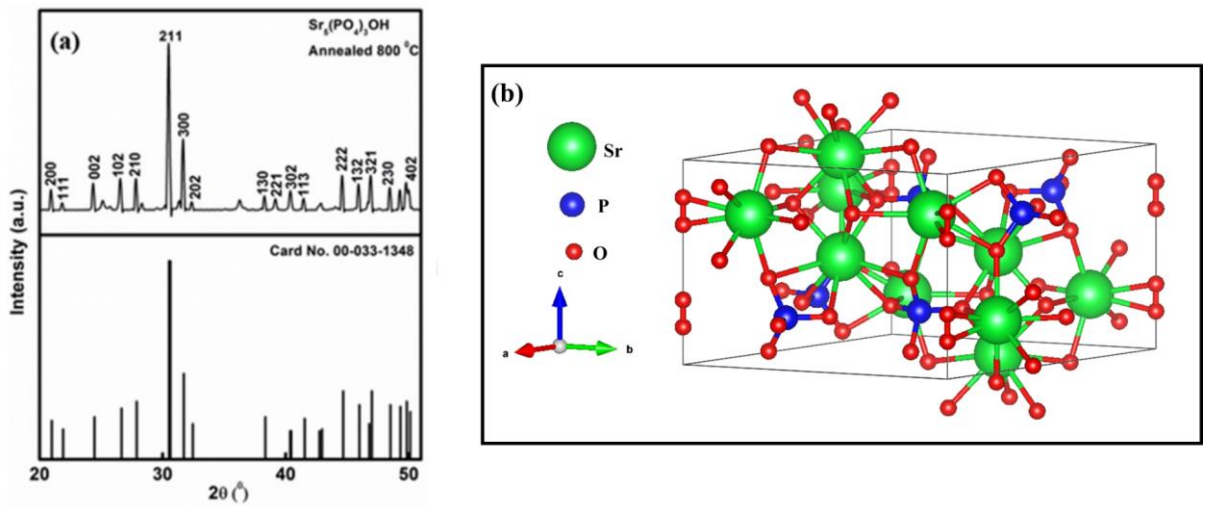

Fig. 1. (*a*) XRD patterns compared with the ICDD Card No. 00-033-1348; (*b*) Crystal structure of the $Sr_5(PO_4)_3OH$ unit cell.

4.2 IR analysis and Particle morphology and chemical composition analysis

SEM micrographs and EDS spectra of $Sr_5(PO_4)_3OH$ co-doped Eu^{3+}/Yb^{3+} phosphor powder are shown in Figure 2 (b-e). The phosphor powders consist of a network of irregular shaped particles, with small bright particles coated on the surface of the larger particles as shown by Fig. 2 (b). The small bright particles are suspected to be the rare earths (Eu^{3+} and Yb^{3+}) ions. The SEM image was taken with backscattered electron detector. The particles with heavy atoms with backscattered electron detector appear brighter, because they are stronger than light particles [9]. Fig. 2 (c) shows the elemental composition of each element in phosphor powders ($Sr_5(PO_4)_3OH:Eu^{3+},Yb^{3+}$) confirming the presence of all the elements in the material. The inset shows the SEM image and the position where the EDS analysis was taken marked with S3 and S4. The bar graph next to it compares the weight % of each element present at the chosen positions. The weight % of rare earths elements (Eu^{3+} and Yb^{3+}) in S3 are 3 and 9%, and in S4 Eu^{3+} and Yb^{3+} is 8 and 16% respectively. This confirms that small bright particles are dominated by Eu^{3+} and Yb^{3+}, while darker particles are dominated by Sr, O, and Ir. The elemental mapping in Fig. 2 (d-e) shows that the elements are uniformly dispersed on the surface of the $Sr_5(PO_4)_3OH:Eu^{3+},Yb^{3+}$ phosphor powder. The Ir (Iridium = 1.977 keV) element present in the spectra and mapping is overlapping with the electron energy of P (Phosphorus = 2.013 keV).

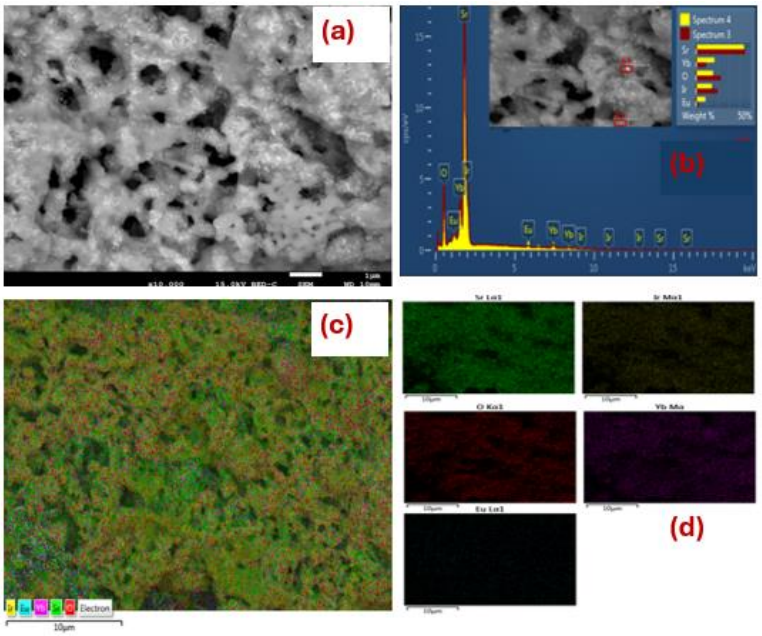

Fig. 2. (a) SEM image, (b) EDS spectrum and (c-d) EDS mapping of $Sr_5(PO_4)_3OH$ co-doped Eu^{3+}/Yb^{3+} phosphor powder.

4.4. UV-Vis spectra: optical and bandgap analysis

The UV-Vis diffuse reflectance spectra and bandgap energy (i) $Sr_5(PO_4)_3OH$, (ii) $Sr_5(PO_4)_3OH:Yb^{3+}$, (iii) $Sr_5(PO_4)_3OH:Eu^{3+}$ and (iv) $Sr_5(PO_4)_3OH:Eu^{3+},Yb^{3+}$ phosphor powders are shown in Fig. 3 (a-b). The $Sr_5(PO_4)_3OH$ spectrum exhibit three prominent bands at 221, 273 and 378 nm nm attributed to interband transition of host and intrinsic defects, respectively [10]. The additional band at 978 nm in $Sr_5(PO_4)_3OH:Yb^{3+}$ spectrum is assigned to $^2F_{7/2}\rightarrow{}^2F_{5/2}$ transition of Yb^{3+} ion [11]. Furthermore, the other bands observed in the visible region of $Sr_5(PO_4)_3OH:Eu^{3+}$ and $Sr_5(PO_4)_3OH:Eu^{3+},Yb^{3+}$ spectra at 391 and 458 nm are attributed to ($^7F_0\rightarrow{}^5L_6$,$^5D_2$) transitions of Eu^{3+} ion, respectively [12]. To estimate the optical energy band gap of the phosphor powders, a plot between F(R) and energy was drawn using Kubelka-Munk (KM) method [13]. By extrapolating the value of the function F(R) =0, the optical energy band gap value of the $Sr_5(PO_4)_3OH$, $Sr_5(PO_4)_3OH:Eu^{3+}$, $Sr_5(PO_4)_3OH:Yb^{3+}$ and $Sr_5(PO_4)_3OH:Eu^{3+},Yb^{3+}$ were estimated to be 5.1, 5.1, 4.7 and 5.2 eV, respectively. The increase in bandgap (blue shift) is due to electrons filling or moving to a high energy state. The excess electrons cause an enlargement of the bandgap, and the process is known as Burstein-Moss effect [11].

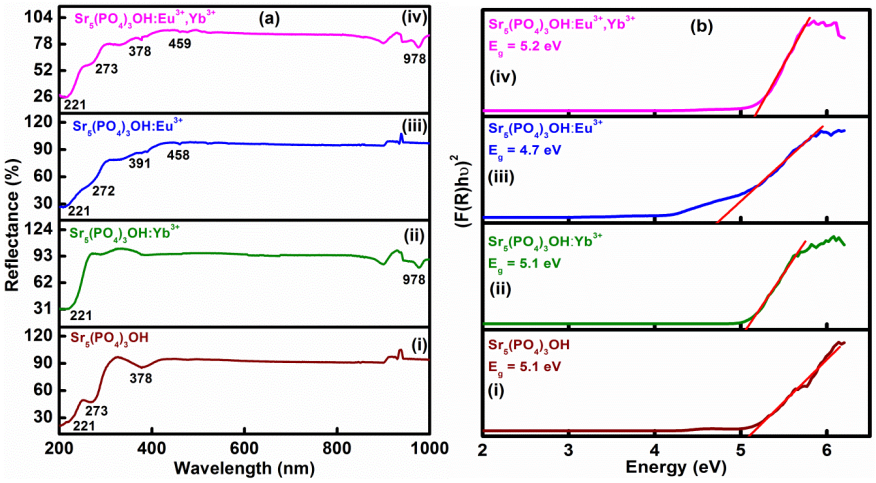

Fig. 3. (a) diffuse reflectance spectra and (b) optical energy bandgap of (i) $Sr_5(PO_4)_3OH$, (ii) $Sr_5(PO_4)_3OH:Eu^{3+}$, (iii) $Sr_5(PO_4)_3OH:Yb^{3+}$ and (iv) $Sr_5(PO_4)_3OH:Eu^{3+},Yb^{3+}$ phosphor powders.

4.5. Photoluminescence spectral analysis.

Fig. 4 (a) presents the excitation and emission spectra $Sr_5(PO_4)_3OH$ with different concentrations of Eu^{3+} (1-7 mol%). The broad band at 245 nm is associated with the charge-transfer band (CTB), arising from the transition of a ligand O^{2-} 2p orbital to the empty states at about $4f^6$ configuration of Eu^{3+} (Eu^{3+}-O^{2-} transition) [14]. The other peaks at 361, 380, 395, 412, 464 and 529 nm are due to direct excitation of the *f-f* transitions of Eu^{3+} ions [15]. The emission peak at 591 nm of the magnetic dipole transition $^5D_0\rightarrow{}^7F_1$ is generated from Eu^{3+} ions, indicating an inversion center site environment for Eu^{3+} ions which correspond to the orange light. The peaks at 613, 652, and 699 nm are corresponding to electric dipole transition ($^5D_0\rightarrow{}^7F_{2,3,4}$) transitions of Eu^{3+}, respectively [16]. The intensity increased with increasing concentrations from 1 to 3 mol % and decreased at a higher concentration due to concentration quenching effects. Upon the excitation at 980 nm, the prominent emission peaks were observed at 476 nm and 522-700 nm attributed to *f-f* transitions of Yb^{3+} ion and other additional peaks may be due to the precursors, respectively, as shown in Fig. 4(b). Under 980 nm excitation, the upconversion luminescence in the red region of Eu^{3+} ion from $^5D_0\rightarrow{}^7F_{j\ (j=1,2,3,4)}$ were detected in $Sr_5(PO_4)_3OH:Eu^{3+},Yb^{3+}$ phosphor powders, as shown in Fig. 4(c). The strongest emission peak is observed at 658 nm attributed to $^5D_0\rightarrow{}^7F_3$ transition of Eu^{3+} ion, and this is due to energy transfer from Yb^{3+} to Eu^{3+} [17]. Figure 4(d) shows the schematic diagram of energy transfer between Eu^{3+} and Yb^{3+}. Through cooperative energy transfer process, Yb^{3+} act as a sensitizer for Eu^{3+}. This suggest that the Eu^{3+} ions are excited due to the presence of Yb^{3+} ions. Consequently, rapid non-radiative relaxation to the metastable $^5D_0$ state can result in a cooperative

energy transfer from a pair of Yb^{3+} ions to a single Eu^{3+} ion, and the red Eu^{3+} emission is observed [18]. Dipole-dipole interaction between pairs of Yb^{3+} and the state of Eu^{3+} ions facilitates the energy transfer. After being stimulated from $^2F_{7/2}$ to $^2F_{5/2}$, two Yb^{3+} ions transfer all their energy to the Eu^{3+} ion's $^5D_1$ state. The Eu^{3+} ion at the $^5D_1$ level undergoes a radiative transition from the various energy states $^5D_0$ to the ground state after relaxing non-radiatively to the luminous level $^5D_0$.

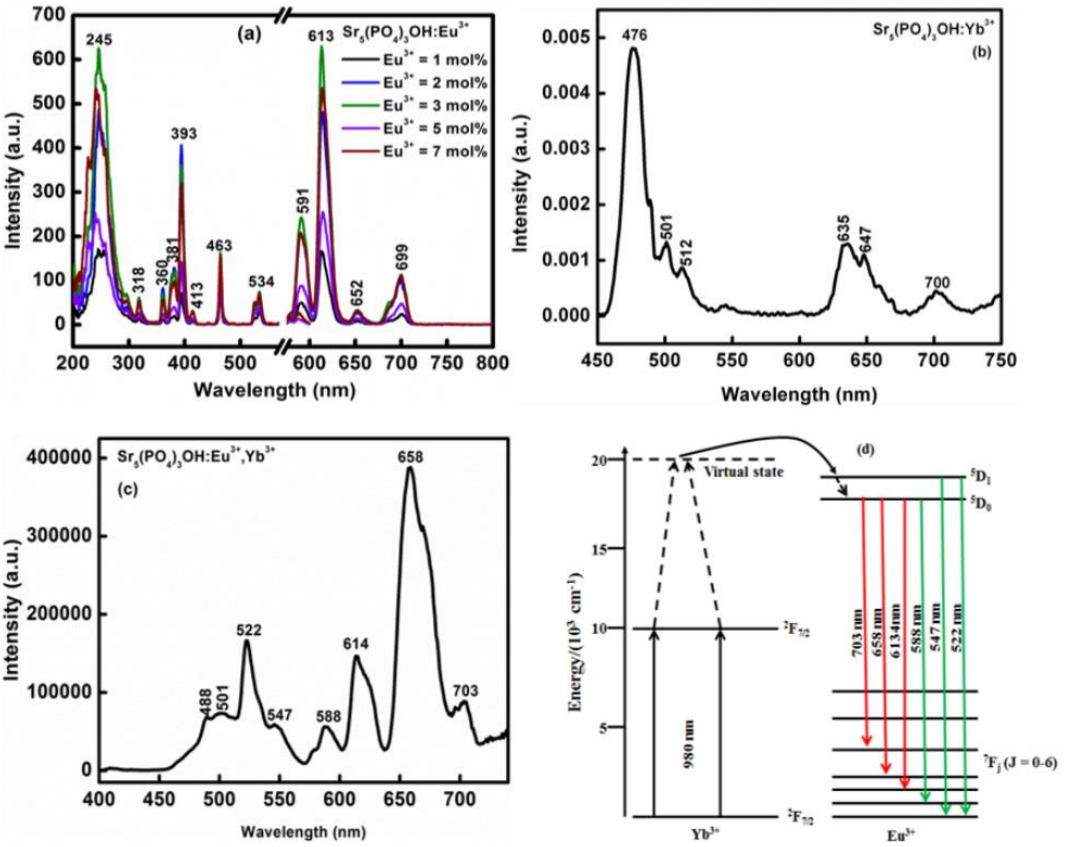

Fig. 4. PL spectral of (a) $Sr_5(PO_4)_3OH:Eu^{3+}$, (b) $Sr_5(PO_4)_3OH:Yb^{3+}$, (c) $Sr_5(PO_4)_3OH:Eu^{3+},Yb^{3+}$ and (d) Energy transfer mechanism.

5. Conclusion

$Sr_5(PO_4)_3OH:Eu^{3+},Yb^{3+}$ phosphor powders were successfully prepared using urea combustion process. The XRD characterization verified the formation of a single phase of $Sr_5(PO_4)_3OH$ when compared to standard data cited by ICDD Card No. 00-033-1348. All of the elements contained in the samples were also confirmed by the EDS spectra. The emission peaks in the 591-699 nm region for the $Sr_5(PO_4)_3OH:Eu^{3+}$ system were attributed to Eu^{3+} transitions. Energy transfer from Yb^{3+} to Eu^{3+} during co-doping with Yb^{3+} increased the red emission peak at 658 nm. Through the use of enhanced red emission, photosensitisers can be activated to treat malignant cells via photodynamic therapy.

6. References

[1] I. Yıldırım , D. Ç. Altındal , A. en Yılmaz, Eu^{3+} doped MB_4O_7 (M= Ca and Sr) nanoparticles for cancer treatment, Journal of Drug Delivery Science and Technology, vol. 105 , pp 106611, 2025, doi: https://doi.org/10.1016/j.jddst.2025.106611

[2] Y.J. Liu, L. Liang, R.R. Wang, J.N. Wu, J.B. Huang, G.M. Cai, J.Y. Si, Crystal structure, electronic structure and thermal stability of new phosphate $Sr_2In(PO_4)(P_2O_7)$, Materials Research Bulletin, vol. 177, pp 112844, 2024, doi https://doi.org/10.1016/j.materresbull.2024.112844

[3] P. Ivanchenko, G. Escolano-Casado, L. Mino, L. Dassi, J. F. Fernandez-Sanchez, G. Martra , J. Gomez-Morales, Structural and surface studies of luminescent Ca/Eu phosphate nanomaterials: From the bulk to surface features, vol. 217, pp 112620, 2022, doi https://doi.org/10.1016/j.colsurfb.2022.112620

[4] M. Eagambaram, K. S. Mani, S. Sahoo, Cobalt intercalated strontium phosphate for cost-effective high-performance supercapacitors, Journal of Energy Storage, vol. 119, pp 116312, 2025, doi https://doi.org/10.1016/j.est.2025.116312
[5] Y. Chen, S.W. Xi, C. Tong, H. hu Tan, L. Xu, N. Li, J.X. Xu, Preparation of $NaYF_4$:Yb^{3+},Tm^{3+}@$NaGdF_4$:Ce^{3+},Eu^{3+} double-jacket microtubes for dual-mode fluorescent anti-counterfeiting, Transactions of Nonferrous Metals Society of China, vol. 30, pp 3333-3346, 2020 DOI: 10.1016/S1003-6326(20)65465-6
[6] Hsiu-Wen Chiena, Chien-Hsin Yang, Min-Ting Tsai, Tzong-Liu Wang, Photoswitchable spiropyran-capped hybrid nanoparticles based on UVemissive and dual-emissive upconverting nanocrystals for bioimaging, Journal of Photochemistry & Photobiology A: Chemistry, vol. 392, pp 112303, 2020, doi: https://doi.org/10.1016/j.jphotochem.2019.112303
[7] P.A. Loiko, G.E. Rachkovskaya,G.B. Zakharevich, A.A. Kornienko, E.B. Dunina, A.S. Yasukevich, K.V. Yumashev, Cooperative up-conversion in Eu^{3+},Yb^{3+}-doped SiO_2–PbO–PbF_2–CdF_2 oxyfluoride glass, Journal of Non-Crystalline Solids, vol. 392-393, pp 39, 2014, doi; https://doi.org/10.1016/j.jnoncrysol.2014.04.004
[8] Katarzyna Szyszka, Marta Kardach, Damian Szymanski, Rafal J. Wiglusz, Synthesis, characterization, and temperature-dependent luminescence of Tb3+-activated and self-activated Sr10(PO4)6Cl2 phosphors, Journal of Luminescence, vol. 275, pp 120788, doi: https://doi.org/10.1016/j.jlumin.2024.120788
[9] P.P. Mokoena, M. Gohain, B.C.B Bezuidenhoudt, H.C. Swart, O.M. Ntwaeaborwa, Luminescent properties and particle morphology of $Ca_3(PO_4)_2$:Gd^{3+}, Pr^{3+} phosphor powder prepared by microwave assisted synthesis, Journal of Luminescence, vol.155, pp 288-292, 2014, doi: https://doi.org/10.1016/j.jlumin.2014.06.058
[10] P.P. Mokoena, I.M. Nagpure, V. Kumar, R.E. Kroon, E.J. Olivier, J.H. Neethling, H.C.Swart, O.M. Ntwaeaborwa, Enhanced UVB emission and analysis of chemical states of Ca 5(PO4)3OH:Gd3+,Pr3+ phosphor prepared by co-precipitation, Journal of Physics and Chemistry of Solids, vol. 75, pp 998-1003, 2014, doi: https://doi.org/10.1016/j.jpcs.2014.04.015
[11] Z. Huang, M. Yi, H. Gao, Z. Zhang, Y.Mao, Enhancing single red band upconversion luminescence of $KMnF_3$:Yb^{3+}/Er^{3+} nanocrystals by Mg^{2+} doping, Journal of Alloys and Compounds, vol. 694, pp. 241-245, 2017, doi: https://doi.org/10.1016/j.jallcom.2016.09.322
[12] J. Chen, W. Zhao, J. Wang, N. Wang, Y. Meng, J. He, X. Zhang, Energy transfer and thermal stability of $K_2Ba(WO_4)_2$: Eu^{3+}, Sm^{3+} phosphors, Ceramics International, vol. 41, pp 11945-11952, 2015, doi: https://doi.org/10.1016/j.ceramint.2015.06.006
[13] Anindya Pala, Purnendu Naskera, Sudeep Paula, Amit Roy Chowdhury, Arijit Sinhaa, Mitun Das, Strontium doped hydroxyapatite from Mercenaria clam shells: Synthesis, mechanical and bioactivity study, Journal of the Mechanical Behavior of Biomedical Materials, vol. 90, pp 328, 2019, https://doi.org/10.1016/j.jmbbm.2018.10.027
[14] C. Shivakumara, R. Saraf, S. Behera, N. Dhananjaya, H. Nagabhushana, Synthesis of Eu^{3+}-activated $BaMoO_4$ phosphors and their Judd–Ofelt analysis: Applications in lasers and white LEDs, Spectrochimica Acta Part A: Molecular and Biomolecular Spectroscopy, vol. 151, pp 141, 2015, doi: https://doi.org/10.1016/j.saa.2015.06.045
[15] V. Naresh, K. Gupta, C.P. Reddy, B.S. Ham, Energy transfer and colour tunability in UV light induced Tm^{3+}/Tb^{3+}/Eu^{3+}: ZnB glasses generating white light emission, Spectrochimica Acta Part A: Molecular and Biomolecular Spectroscopy, vol. 175, pp 43, 2017, doi: https://doi.org/10.1016/j.saa.2016.12.023
[16] El Mahdi Bouabdalli, Mohamed El Jouad, Samira Touhtouh, Nathalie Gaumer, El Kebir Hlil, Abdelowahed Hajjaji, The effect of europium on structural properties, photoluminescence behavior, and Judd-Ofelt analysis in strontium phosphate glasses for photonic applications, Radiation Physics and Chemistry, vol. 226, pp 112238, 2025, doi: https://doi.org/10.1016/j.radphyschem.2024.112238
[17] H. Rahimian, H. Mokhtari, S.P. Shirmardi, Improvement of Eu3+ emissions in oxyfluoride glass and nano glass-ceramic by electron beam irradiation, Journal of Luminescence, vol. 187, pp 535, 2017, doi: https://doi.org/10.1016/j.jlumin.2017.03.025
[18] H. Xia, J. Feng, Y. Ji, Y. Sun, Y. Wang, Z. Jia, C. Tu, 2.7 μm emission properties of Er^{3+}/Yb^{3+}/Eu^{3+}: $SrGdGa_3O_7$ and Er^{3+}/Yb^{3+}/Ho^{3+}: $SrGdGa_3O_7$ crystals, Journal of Quantitative Spectroscopy & Radiative Transfer, vol. 173, pp 7, 2016, doi: https://doi.org/10.1016/j.jqsrt.2015.12.018